# Enhancement of the Open National Combustion Code (OpenNCC) and Initial Simulation of Energy Efficient Engine Combustor

Kenji Miki [*], Jeffrey Moder[†], Meng-Sing Liou [‡]
*NASA Glenn Research Center,*
*Cleveland, Ohio 44135, USA*

**In this paper, we present the recent enhancement of the Open National Combustion Code (OpenNCC) and apply the OpenNCC to model a realistic combustor configuration (Energy Efficient Engine ($E^3$)). First, we perform a series of validation tests for the newly-implemented advection upstream splitting method (AUSM) and the extended version of the AUSM-family schemes ($AUSM^+$-up). Compared with the analytical/experimental data of the validation tests, we achieved good agreement. In the steady-state $E^3$ cold flow results using the Reynolds-averaged Navier-Stokes(RANS), we find a noticeable difference in the flow fields calculated by the two different numerical schemes, the standard Jameson-Schmidt-Turkel (JST) scheme and the AUSM scheme. The main differences are that the AUSM scheme is less numerical dissipative and it predicts much stronger reverse flow in the recirculation zone. This study indicates that two schemes could show different flame-holding predictions and overall flame structures.**

## I. Introduction

Designing high-pressure turbines (HPTs) for peak temperatures at the combustor exit decreases cycle efficiency since excess cooling air is required, while designing HPTs for the mean exit-temperature at the combustor exit may reduce turbine life since excessive metal temperatures may occur at local hot spots along turbine blades. Improved modeling of combustor-turbine interactions can provide strategies for conditioning the combustor exit flow or optimized cooling strategies for HPT, which provides increased engine cycle efficiency and improves turbine blade life and overall gas turbine durability. Future propulsion systems will be of increasingly higher bypass ratio from larger fans combined with much smaller cores, which increases the importance of understanding core engine component interactions, such as combustor-turbine interactions. This work represents the first steps in a longer-term effort to investigate and quantify the effects spatial and temporal temperature non-uniformity of the combustor flow field on the high-pressure turbine performance using high-fidelity CFD simulations.

Although there have been significant improvements recently in the field of computational fluid dynamics (CFD), the current maturity of the CFD capability of modeling a gas turbine and the relevant physics involved is not fully satisfactory. This is due to the fact that a gas turbine combustor is a complex system coupled with multi-physical phenomena, i.e. atomization, transport, vaporization and combustion, all of which are closely connected to turbulence. Design of gas-turbine combustors typically uses RANS during initial design cycles and Large Eddy Simulation (LES) for final design evaluation. RANS provides averaged solutions with relatively low computational cost (several hours for modeling a typical gas combustor). On the other hand, LES can provide an improved description of unsteady features, including turbulence and mixing, in contrast to traditional RANS methods.[1] LES also provides a tool to predict unsteady phenomena, such as flame stability, combustion dynamics, and combustor-turbine interaction (hot-streaks), all which are of our ultimate interest.

[*]Postdoctoral Researcher, AIAA Member
[†]Research Aerospace Engineer, AIAA Member
[‡]Senior Technologist, AIAA Fellow

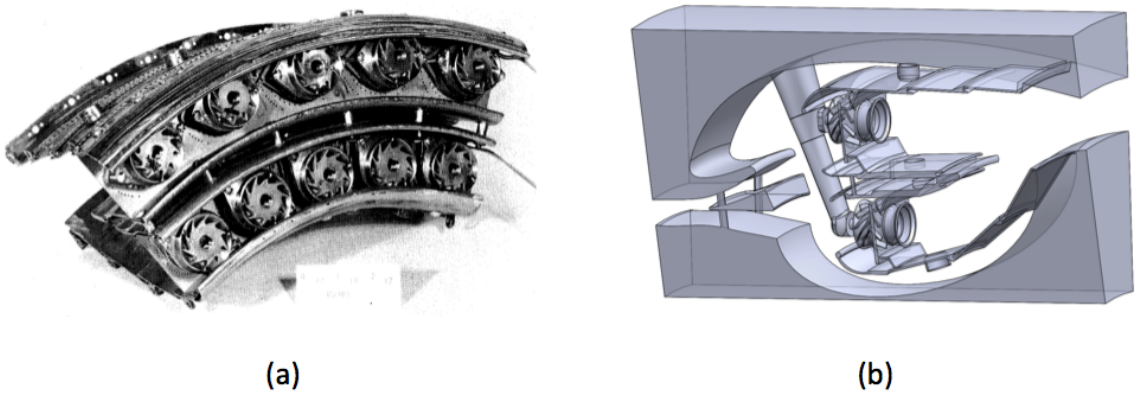


**Figure 1. (a) Five-cup $E^3$ sector test hardware[12] and (b) one-cup CAD geometry.**

At the National Aeronautics and Space Administration (NASA) Glenn Research Center, we have been developing a high-fidelity three-dimensional unsteady flow solver (OpenNCC), which is a publicly releasable version of the National Combustion Code (NCC).[2] A dual time-stepping approach is combined with a 4-stage explicit Runge-Kutta time-integration scheme to achieve the second-order accuracy in time. OpenNCC is capable of using unstructured meshes and has a massively parallel computing capability, with which we are able to simulate different types of combustors (e.g., Lean Direct Injection (LDI) combustion) related to a variety of NASA missions. For more than two decades, the team has continuously updated the NCC (and OpenNCC) by adding more physical modules, such as a turbulence module (nonlinear $k-\epsilon$ model[3]), combustion modules (reduced chemical kinetic, low dimensional manifold), a spray module,[4–6] and a joint probability density function for species and enthalpy. There are two numerical schemes implemented in OpenNCC: the standard Jameson-Schmidt-Turkel (JST) scheme and Roe's upwind scheme. Recently, we implemented the advection upstream splitting method (AUSM)[7] and the extended version of the AUSM-family schemes ($AUSM^+$,[8] $AUSM^+$-up[9]). The uniqueness of this type of scheme is that it does not have any computationally expensive matrix operation nor any differentiation of fluxes causing any numerical errors, yet it maintains accuracy. Another important feature is that there are not modeling parameters that need to be adjusted for applications (for instance, in the JST scheme, the second-order and fourth-order artificially dissipation coefficients need to be tuned, and the choice of these parameters are closely related to the numerical stability and then the final results). We have performed a series of validation tests for the newly-implemented AUSM scheme, such as skin friction at the laminar/turbulence flat plates and heat flux of the highly-loaded turbine guide vane at the Von Karman Institute (VKI), and methane-air reacting flow in a non-swirling coaxial jet combustor at the United Technologies Research Center (UTRC).[10]

This paper represents a first step toward the ultimate objective of tightly-coupled unsteady simulations of combustor-turbine interactions for realistic combustor and turbine geometries. To advance our current capabilities, we start with the non-proprietary combustor and high-pressure turbine designs from the Energy Efficient Engine ($E^3$) program[11] (using the General Electric combustor and HPT designs). While only the $E^3$ combustor geometry is considered in this paper, we plan to eventually simulate the $E^3$ HPT geometry and the coupled $E^3$ combustor-HPT geometry (shown in Figs. 1 and 2, respectively). The $E^3$ was intensively investigated in the mid-1970s and 1980s and set a historically important milestone toward more fuel efficient jet engines that meet the emission requirements. The relevant technologies that emerged from this program have since been widely used in current commercial engines.

The $E^3$ is the double-annular and compact combustor. The fuel injected from 30 fuel nozzles and the swirling air are efficiently mixed and combusted in a short distance. At a low power condition, only the outer dome is fueled, and a rich combustion zone is formed. At a high power condition, both domes are fueled and a large amount of airflow is introduced into the inner dome annulus, creating a very lean combustion zone. Large dilution holes at the center body and inner/outer liners are designed in such a way that the cold airflow immediately mixes with the hot product, suppressing the further NOx formation. A detailed explanation of $E^3$ can be found elsewhere.[12]

Although this type of combustor is designed for efficient fuel/air mixing and a relatively uniform exit temperature profile, temporary severe non-uniformity of temperature (i.e., hot-streaks) at the combustor exit is inevitable even for the latest and most advanced combustors. These hot streaks can cause local hot spots on the blade surfaces of high-pressure turbine stages, which is a potential source of blade life reduction. In order to improve understanding of these effects, numerous experimental and numerical studies have been carried out. However, due to the aforementioned coupled multi-physical phenomena, the numerical modeling is still not mature enough for a full understanding of the combustor-turbine interactions (and formation of hot-streaks). Thus, our goal is to enhance the current model capability of OpenNCC for this purpose.

The layout of the paper is as follows. In Section 2, we briefly explain the OpenNCC and the current capability and subsequently show a series of validation works for the newly implemented numerical models. In Section 3, we show some preliminary work applying the current code to the $E^3$ and investigate the three-dimensional flow feature inside the combustor. Our conclusions are summarized in Section 4.

## II. Numerical Models

A brief explanation of OpenNCC is provided in this section. OpenNCC is the releasable version of the NCC, which has been continuously updated for more than two decades at NASA Glenn Research Center (GRC). It is a state-of-the-art code equipped with a comprehensive combustion model, a turbulence model (cubic non-linear $k-\epsilon$ model with the wall function), and a numerical simulation and spray model (Lagrangian liquid phase model). Many previous papers and presentations (e.g.,[2,3,14–17]) have shown that OpenNCC (as well as NCC) has facilitated the combustion CFD in the development/design of the combustion technology at NASA-GRC. However, as with any other CFD code, there is a need to continue updating the code through verification and validation (V&V). Our experimental combustion group at NASA-GRC provides the validation data to improve the OpenNCC (e.g.,[18,19]). For the numerical and mesh capability, OpenNCC is designed for unstructured grids (i.e., any mix of three-dimensional elements: hexahedral and tetrahedral mesh), and massively parallel computing (with almost perfectly linear scalability is achieved for non-spray cases up to 4000 central processing units). In addition, the adaptive mesh refinement option is recently implemented.[20] For low-speed flow, pre-conditioning is used for better convergence. The combination of these unique features gives OpenNCC an advantage in the investigation of a variety of combustor/injector applications.

## III. Validation Test

As a part of the continuous improvement efforts of OpenNCC, we recently implemented the AUSM[7] and the other extended version of the AUSM-family schemes ($AUSM^+$,[8] $AUSM^+$-up[9]) and the turbulence transition model.[21] The AUSM scheme is particularly attractive for its very simple formulation (i.e., computationally cheap), no *ad hoc* model parameters, and great accuracy. Also, this simple formulation easily facilities the addition of other variables. The key idea is to split the inviscid flux, $\mathbf{F}$, into the convective $\mathbf{F_c}$

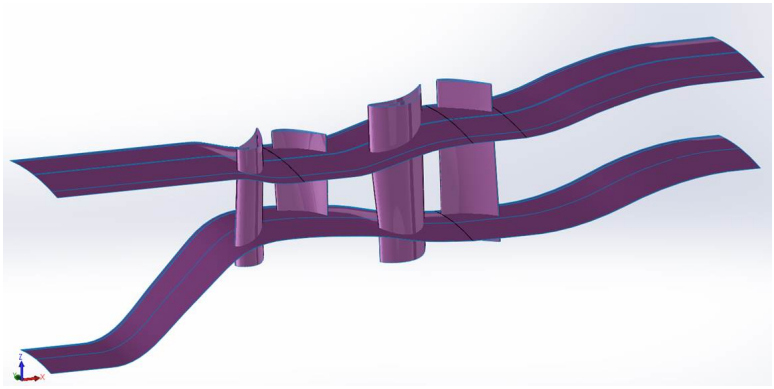

**Figure 2. CAD Geometry of high-pressure turbine stages of $E^3$ (based on geometry data[13]).**

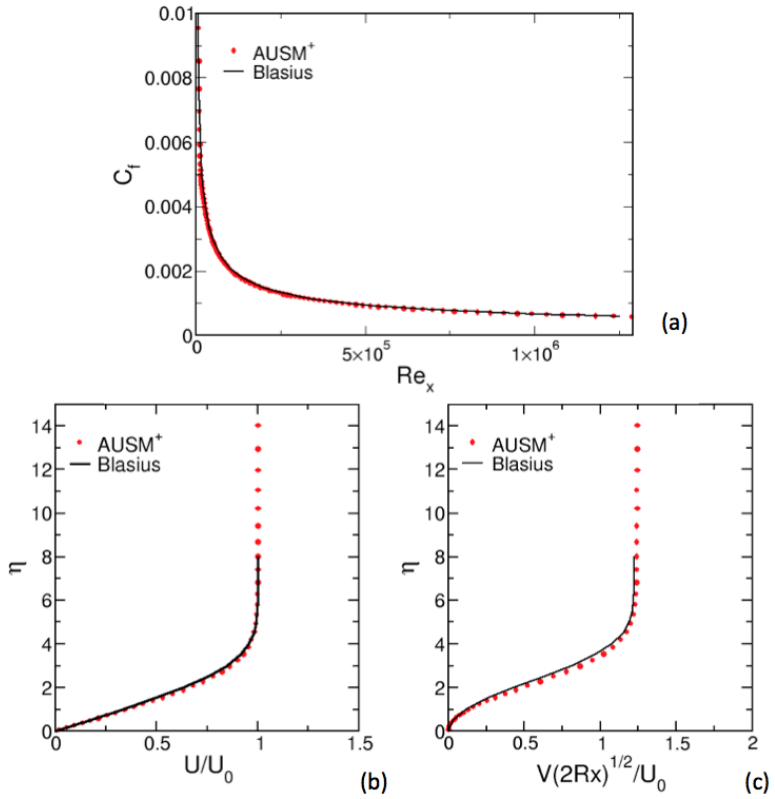


**Figure 3. Skin friction (top) and velocity profiles (bottom) for the laminar flat plate.**

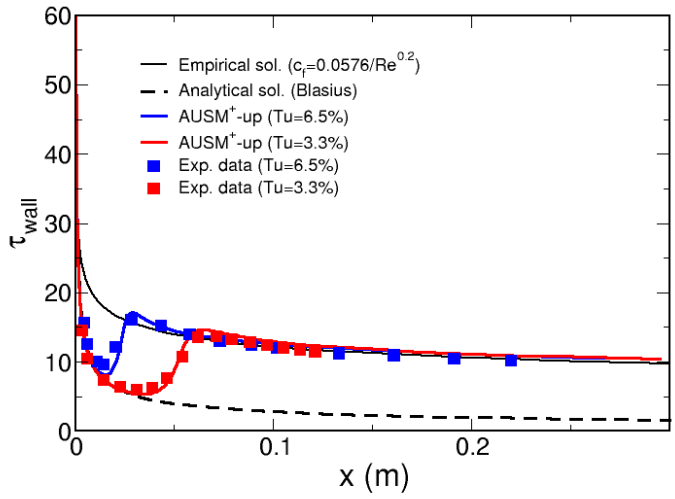


**Figure 4. Predicted wall friction on the turbulent flat plate and the experimental data.**

and pressure $\mathbf{P}$ terms,

$$\mathbf{F} = \mathbf{F_c} + \mathbf{P} \tag{1}$$

where $\mathbf{F_c}$ and $\mathbf{P}$ are $(\rho, \rho u, \rho h_t)$ and $(0, p, 0)$ for the one-dimensional system. $\rho$, $u$ $h_t$ and $p$ are density, velocity, total enthalpy and pressure. Then, the numerical approximations of the cell interface Mach number, the sound speed and the pressure are evaluated by the right and left cell variables. The extension of the high-order scheme can be done based on the MUSCL scheme.[22] Please see other references for a detailed explanation of AUSM (e.g.,[7–9]). A series of validation of the newly implemented AUSM scheme of the OpenNCC has been performed. The turbulence transition model developed by Liou and Shih[21] on the platform of two equation models is also implemented. The model is based on the experimental observation that the transition takes place in the highly intermittent flow, so they introduce the intermittency correction function, $\gamma$ which reflects the peak disturbance energy. The implementation of the model into the OpenNCC is fairly straightforward; however, finding the peak disturbance energy in the wall normal direction within the massively parallel computing system should be done with care.

### A. Laminar/Turbulence Flat Plate

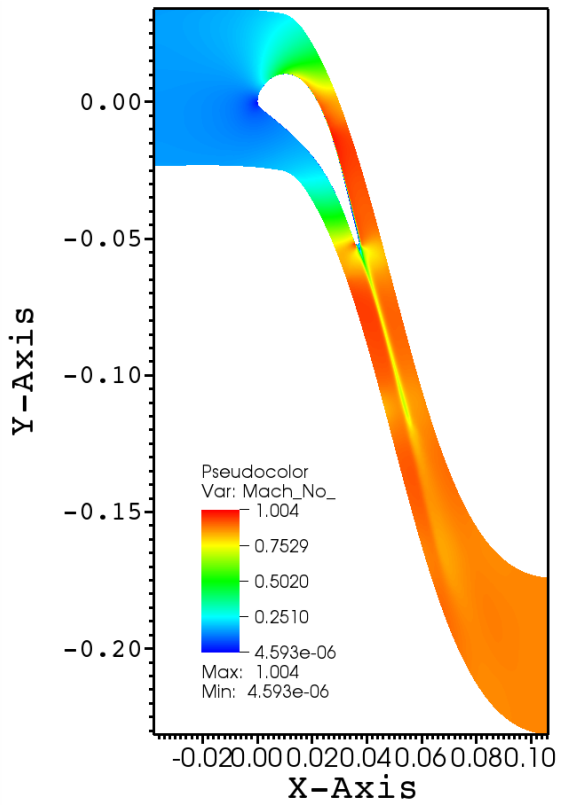


**Figure 5. Contour of Mach number of VKI vane for MUR 45.**

The first case is to simulate the laminar flow over the flat plate. The results are compared with the Blasius solutions. The single block, two-dimensional structured mesh is generated by Cubit, a software toolkit developed at Sandia National Laboratories. The grid density is 128 × 64. The inflow and outflow condition is: $\mathrm{Ma}_{in} = 0.2$, $\mathrm{T}_{in} = 300$ [K], and $\mathrm{p}_{out} = 101{,}352$ [pa]. The wall is treated as an adiabatic and non-slip wall. The resulting skin friction, u and v velocity profiles at the exit are compared with the Blasius solution (see Figs. 3 (a)-(c)). Excellent agreement is achieved.

The second validation case is to predict the skin friction of the turbulent flow over the flat plate. The experimental and empirical fit ($C_f = 0.0576/Re^{0.2}$ are available. Two single blocks, two-dimensional structured meshes (grid densities are 256 × 128 and 512 × 256) are generated by Cubit, and we refine the mesh to adequately resolve the flow in the vicinity of the wall. These two meshes are used to check the grid dependency of the result. There are two operating conditions to test: $Tu = 3.3$ % and $Tu = 6.5$ %. The mixing length is chosen so that $\mu_t/\mu = 10$. Fig. 4 shows the predicted wall shear stress using the 256 × 128 grid. There is good agreement in the data with respect of the magnitude as well as the transition location.

### B. VKI Heat Flux

The third validation test is to investigate the flow around the highly loaded turbine guide vane. The data was acquired at the Von Karman Institute (VKI), and the detailed test configuration and operating conditions are provided by the reference.[23] They measured the velocity distribution by means of static pressure tappings and the wall heat flux by platinum thin films. Experimental uncertainties are also provided, pressure: ±0.5 % and heat flux: ±5 %. Here, we pick three free stream conditions, MUR45, MUR129 and MUR235 (see Table. 1) Note the inflow total temperature is not provided for MUR45. Thus, we estimate 410 [K] based on other experimental conditions.

Figure 5 shows the contour plot of the Mach number for MUR45 (laminar calculation). We can see that the flow reaches supersonic speed at the suction side and then gradually decelerates toward the trailing edge. The current mesh allows the wake region to extend well in the computational domain without crossing the periodic wall (bottom and top walls), which minimizes the numerical errors. We observe the expansion on

**Table 1. List of experimental free stream condition.[23]**

| Test number # | $p_{total}$ (bar) | $T_{total}$[K] | $Mis_{out}$ | $Re_{out}$ | Free stream turb. [%] |
|---|---|---|---|---|---|
| MUR45 | 1.475 | - | 0.875 | $10^6$ | - |
| MUR129 | 1.849 | 409.20 | 0.840 | $1.1352 \times 10^6$ | 0.8 |
| MUR235 | 1.828 | 413.3 | 0.927 | $1.1521 \times 10^6$ | 6.0 |

the pressure side in the vicinity of the trailing edge due to the large curvature. Figures 6 (a) and (b) show the pressure and the isentropic Mach number (Mis) with the experimental data (black circle) for MUR45. There are reasonably good agreements obtained, except the trailing edge region where we need to refine the mesh further more. Figures 7 (a) and (b) show the wall heat flux for MUR129 and MUR235. The region with negative X/C indicates the pressure side. For MUR129, the result using the laminar model agrees well with the experimental data and the one from Gourdain *et al.*[24] For MUR235 (see Fig. 7 (b)), both our model and Gourdain *et al.* (RANS) are similar to each other and predict much less heat flux at the laminar region than the data. In fact, Gourdain shows that using the high fidelity model (i.e., LES) performs better. Note that MUR235 is the most challenging case in the sense that there are transitions from laminar to turbulence as well as weak shock.

### C. UTRC Non-Swirling Coaxial Jet Combustor

The fourth validation test is to simulate the coaxial jet combustor experiment conducted by Spadaccini *et al.*[10] This configuration is relatively simple, but similar to a gas turbine combustor in the sense that in both cases, the flame is held by the recirculation zone. Detailed measurements (species, temperature and velocity profiles at different axial locations) are available.

Figures 8 (a)-(c) show the computational domain and meshes. All the grids are structured and the mesh count is about 370,000.[25] The inflow condition of the fuel and air are summarized in Table. 2. Figure 9 shows the axial velocity (left) and temperature (right) contours using two different numerical schemes, the JST scheme (top row)[25] and the AUSM scheme (bottom row). In both cases the k-$\epsilon$ turbulent model is used, and the chemistry-turbulence interaction model is turned off (i.e., the reaction rates are evaluated by the mean temperature). Compared with those utilizing the JST scheme, the AUSM scheme predicts a much stronger reverse flow, and as a consequence, the hot product stays upstream and the fuel stream expands more in the radial direction. We observe that the cold fuel core predicted by the JST scheme remains downstream in the temperature profile. Figs. 10 (a)-(e) and Figs. 11 (a)-(d) show comparisons of the axial velocity and temperature between the predictions by the AUSM scheme (red solid line) and the experimental data

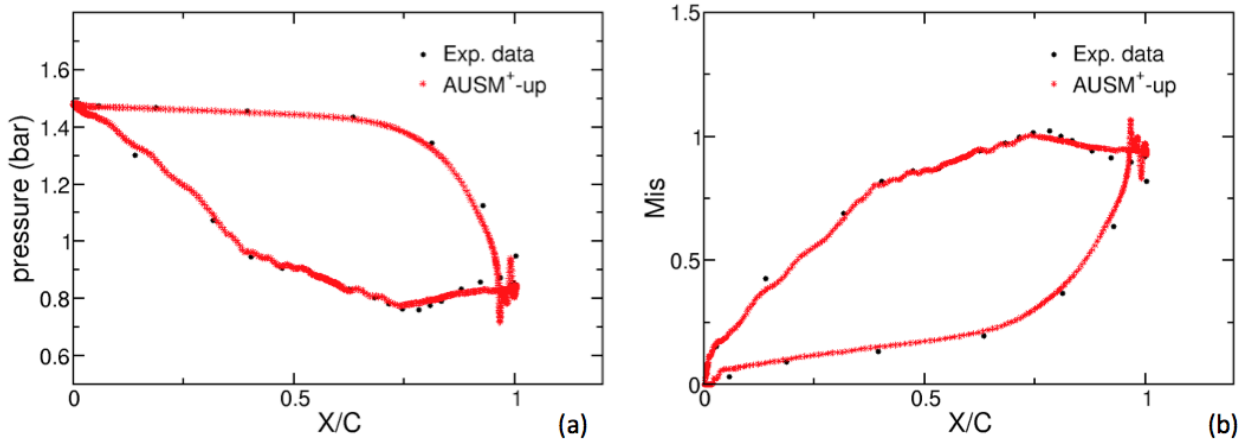


**Figure 6. (a) Pressure and (b) Mach number profiles for MUR 45.**

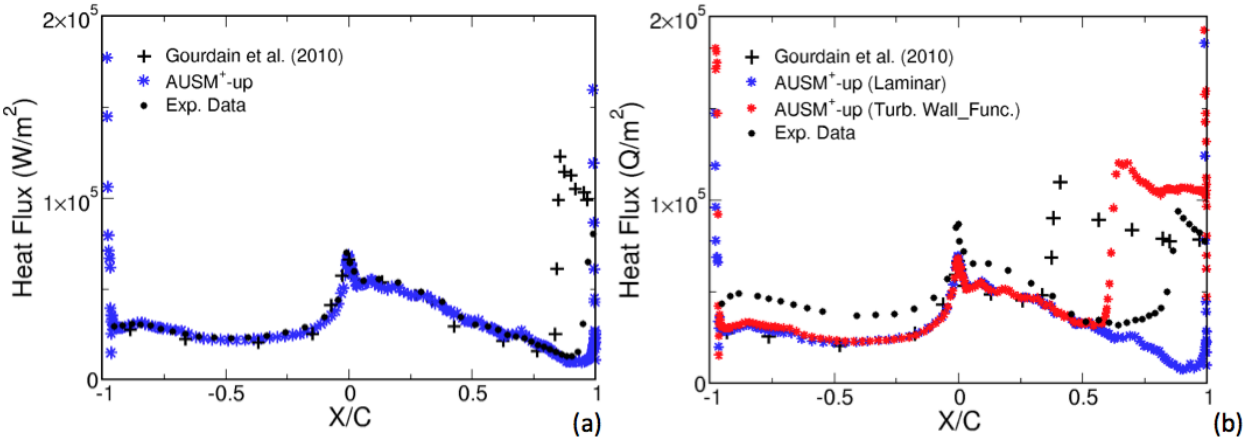


**Figure 7. Heat flux at pressure side (X/C<0) and suction side (X/C>0) for MUR45 (a) and MUR235 (b). The circle and plus are from[23] and.[24]**

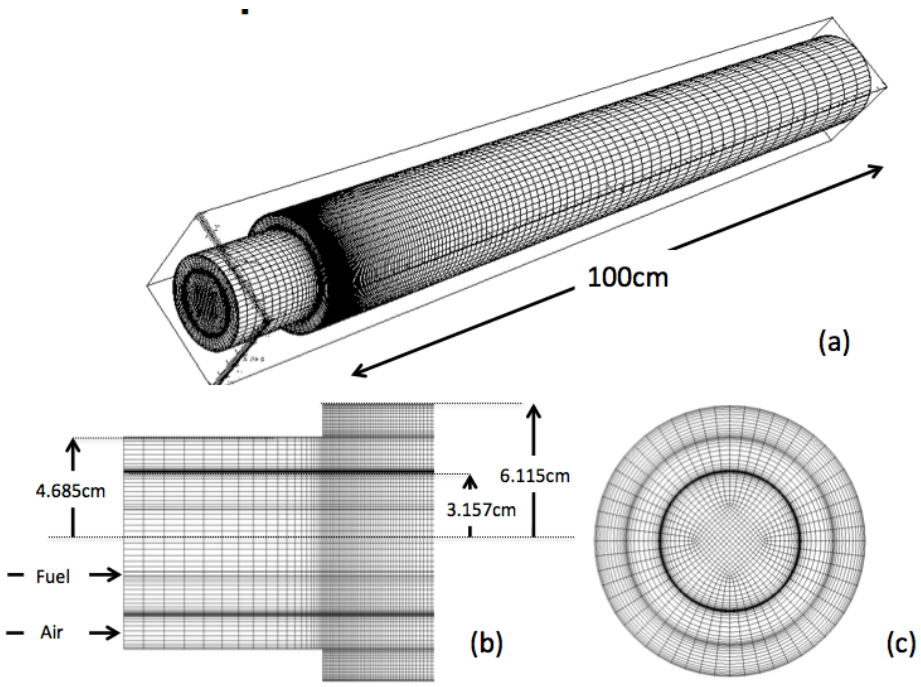


**Figure 8. Geomtry of the coaxial jet combustor and meshes.[25]**

**Table 2. Experimental setup of UTRC non-swirling coaxial Jet combustor.[10]**

| gas | Temperature [K] | Mass flow rate [kg/s] | Velocity [m/s] |
|---|---|---|---|
| Air | 750 | 0.137 | 29 |
| Fuel ($CH_4$) | 300 | 0.0072 | 0.9 |

(triangle)[10] at different axial locations. From Fig. 11 (a), we can see that the hot product stays upstream in a way similar to that which is as predicted by the AUSM scheme. Overall, reasonably good agreement has been achieved.

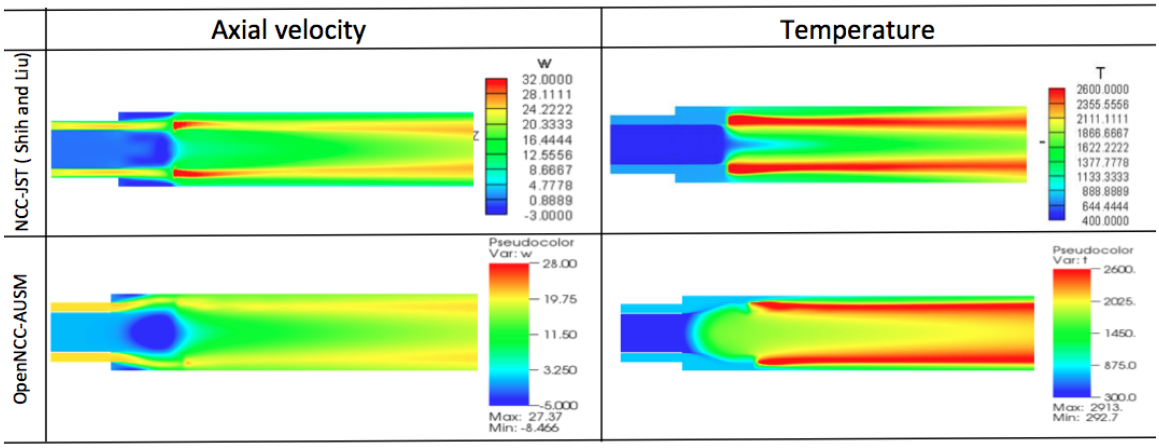


**Figure 9. Contour of axial velocity (left) and temperature (right) using two different numerical schemes: JST (top)[25] and AUSM (bottom)**

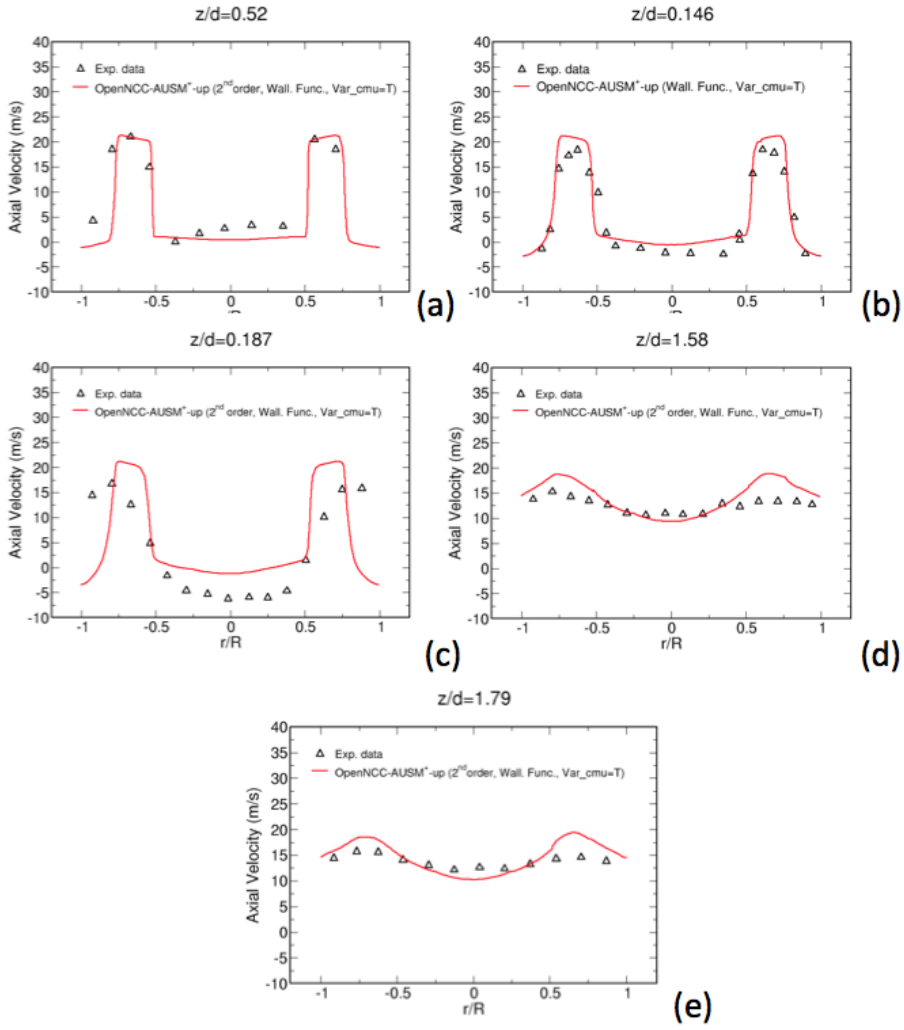


**Figure 10. Axial velocity profile at five different axial locations: z/d = 0.52, 0.146, 0.187, 1.58 and 1.79. The solid red line and triangle are the numerical prediction and the experimental data.[10]**

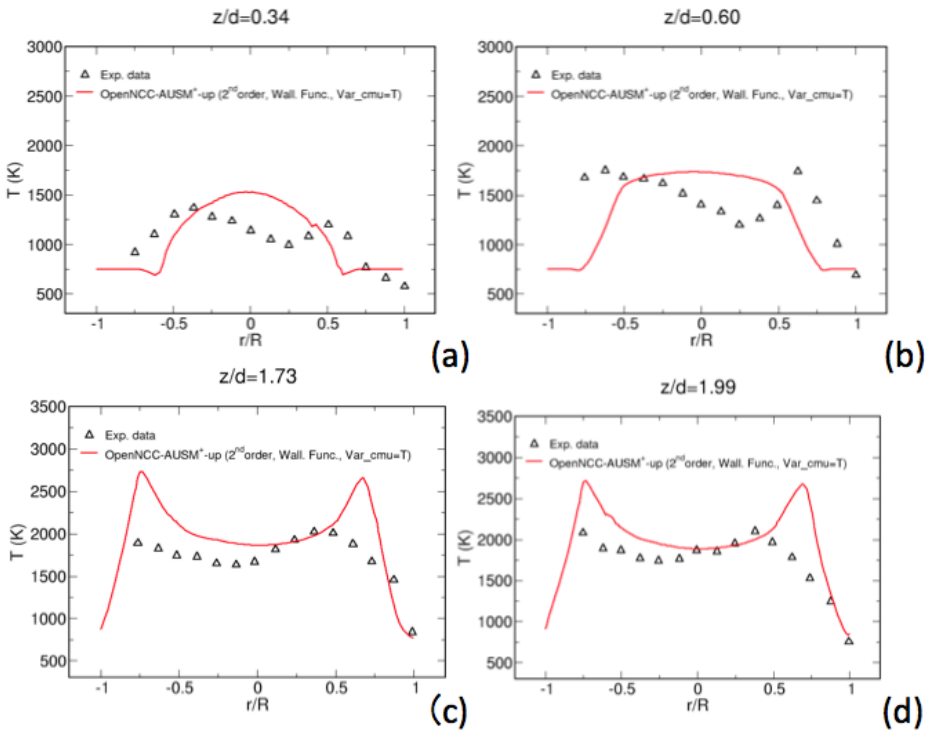


**Figure 11. Temperature profile at four different axial locations: z/d = 0.34, 0.60, 1.73 and 1.99. The solid red line and triangle are the numerical prediction and the experimental data.[10]**

## IV. E$^3$ Combustor

In this section, we apply the OpenNCC to simulate the E$^3$ combustor and show some preliminary results using the RANS.

### A. Numerical Setting and Boundary Condition

For this calculation, thanks to the massively parallel computing capability of OpenNCC, we routinely use 960 processors of Pleiades at NASA Advanced Supercomputing facility. The tetrahedral mesh is generated by Cubit. The total mesh count is about 9.5 million. (Note that we are aware that using tetrahedral mesh for an internal flow should be done with care since it is numerically dissipative and not good at capturing the boundary layer). In future works, we would like to turn on the adaptive mesh refinement option in OpenNCC.[20]

For illustration purposes of the enhanced OpenNCC capability, all results shown here are obtained by using the RANS with the low-Mach preconditioning. The turbulence model is the nonlinear $k-\epsilon$ model,[3] and two types of numerical schemes are used, the JST scheme and the AUSM scheme. In the JST scheme, we set the second and forth artificial dissipation coefficients to be 0.02 and 0.06, respectively. The E$^3$ experimental setup is shown in Table. 3 . The sea level takeoff condition (SLTO) is the most severe condition during the engine operation cycle. The pressured air (P3 = 2.52 [atm]) is introduced from the left boundary (A1) in Fig. 12. The air goes around the diffuser splitter vane, and some portion of air (S1) is diffused into the strut cavity and routed through the hollow strut passage into the cooling circuit. In the reacting flow case, both the main and pilot domes should be equally fueled (F1 = F2 = 0.00182 [kg/s]). There are several cooling airflow (A2 - A14) at the outer/inner liners and the center body surface. We treat them as source/suction terms (i.e, no grids to resolve the cooling holes), and the mass flow rates are summarized in Table. 4.

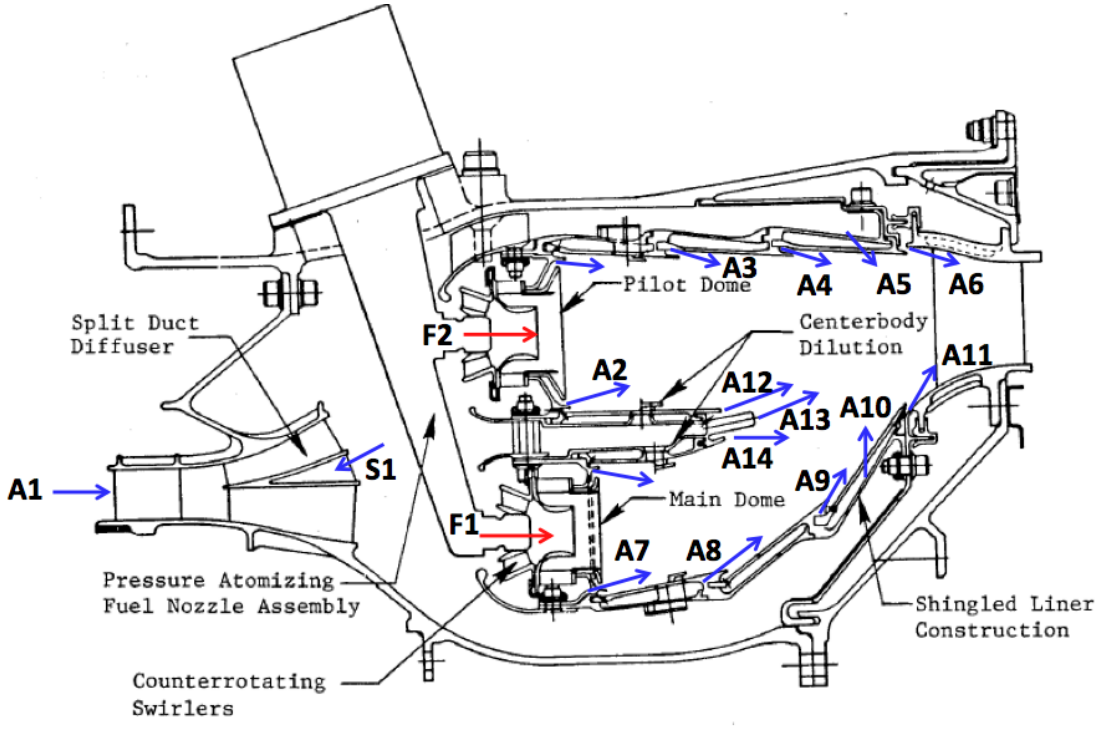


**Figure 12. Cross section of the sector E$^3$ combustor and injectors.**

**Table 3. E$^3$ experimental setup.[12]**

| | P3 [atm] | T3 [K] | W3 [kg/s] | $Wf_{total}$ [kg/s] | f/a | $Wf_{pilot}/Wf_{total}$ | $T_{fuel}$ [K] |
|---|---|---|---|---|---|---|---|
| SLTO | 2.52 | 720 | 0.26 | 0.00364 | 0.014 | 0.5 | 520 |

## B. Cold Flow Comparison

In this subsection, we show the cold flow (the domes are not fueled) results using the JST scheme and the AUSM scheme. The contours of gage pressure, u-velocity, v-velocity and w-velocity at the mid-plane are shown in Figs. 13 (a)-(h). Both models are able to qualitatively capture the important features of the internal airflow inside the combustor in a similar way, such as the central recirculation zone (CRZ), high pressure region behind the domes, swirling flows, strong cross airflow from the dilution holes, and cooling air from liners covering the combustor liner. The predicted pressure drop across the combustor liner is 5.1% (main) and 4.7% (pilot), which is consistent with the designed pressure drop, 5%. The CRZ, which is formed due to the breakdown of a highly-swirled flow, plays a critical role in holding the flame in this type of a swirl stabilized combustor and is often associated with the low pressure region in the vicinity of the fuel nozzle, the so-called precessing vortex core (PVC). The inherent unsteady feature of the PVC significantly impacts the combustion dynamics and emission.[26,27] Even though the presence of the PVC can improve the mixing because of the creation of larger turbulent scales, it is important to suppress the PVC in order to reduce the combustion dynamics, which can lead to catastrophic failure of the combustor. In the contours of u-velocity and v-velocity (Figs. 13 (c) - (f)), it is found that there is a large CRZ (blue region) located between the dome and the dilution flows, where the flame is supposed to be held in a reacting flow case. The wake region behind the dilution airflow coming from the center body can be a potential region where some NOx is formed. At the end of the inner/outer liners, the flow field becomes relatively uniform. In the w-velocity profiles (Figs. 13 (g) - (h)), a strong swirling flow around the fuel nozzles is observed. It is found that the strength of the swirling flow is slightly stronger in the main dome than in the pilot dome, which

**Table 4. Flow area distribution[12] (* Note for the cold flow calculation, both domes are not fueled).**

| Aame | Index | Gas | Mass flow rate [kg/s] |
|---|---|---|---|
| Inflow | A1 | Air | 0.26 |
| Main dome | F1 | Fuel | 0.00182* |
| Pilot dome | F2 | Fuel | 0.00182* |
| Diffuser Bleed | S1 | Air | - 0.018 |
| Pilot splash plate cooling | A2 | Air | 0.0104 |
| Outer liner cooling 1 | A3 | Air | 0.0053 |
| Outer liner cooling 2 | A4 | Air | 0.0053 |
| Outer liner trim cooling | A5 | Air | 0.0018 |
| Outer liner cooling 3 | A6 | Air | 0.0024 |
| Main splash plate cooling | A7 | Air | 0.0116 |
| Inner liner cooling 1 | A8 | Air | 0.0096 |
| Inner liner cooling 2 | A9 | Air | 0.0056 |
| Inner liner trim cooling | A10 | Air | 0.0018 |
| Outer liner cooling 3 | A11 | Air | 0.0024 |
| Centerbody outer cooling | A12 | Air | 0.0018 |
| Centerbody mid cooling | A13 | Air | 0.0024 |
| Centerbody Inner cooling | A14 | Air | 0.0024 |

should be related to the fact that the airflow coming from the diffuser is aligned to the main dome (i.e., the pressure in the outer liner is higher). Also, the AUSM scheme predicts a higher magnitude of w-velocity (stronger swirling flow) than the JST scheme does.

Figures 14 show the Mach number contour (blue: Mach = 0 and green: Mach = 0.2) at two different axial locations (x=0.175 [m] and 0.18 [m] ) just downstream of the pilot dome. We observe that the swirling flow attenuates more quickly for the JST scheme due to the numerically dissipative nature. The same conclusion is drawn from the Mach number contour near the main dome (not shown).

The three-dimensional features (iso-surface of the u-velocity (green: -30 [m/s]) and v-velocity (red:-100 [m/s], and blue: 100 [m/s]) of the predicted PVC and the dilution airflow are shown in Figs. 15 (a) JST scheme and (b) AUSM scheme. For the AUSM scheme, the CRZ (green) is much larger and extends upto the location where the dilution airflows meet. In contrast, the JST scheme predicts a much smaller CRZ, and the CRZ and the dilution airflows are weakly interacted. This is consistent with what we see in the w-velocity contour in Figs. 13 (g) - (h).

In order to investigate the CRZ and PVC, we perform the quantitative comparison of u-velocity and pressure profiles in the vicinity of the main dome and pilot dome. Figs. 16 (a) and (b) show the u-velocity profiles in the axial direction (please see the inserted figure). We compare the location where the profile reaches u-velocity = -30 [m/s] and observe that the AUSM scheme (black circle) shows a much larger CRZ than what the JST scheme (red circle) does. More importantly, the maximum value of the reverse flow obtained by the AUSM scheme is -60 [m/s] (main) and -53 [m/s] (pilot), which are much stronger than the ones by the JST scheme (-40 [m/s] (main) and -38 [m/s] (pilot)). Under the same numerical setting (e.g., mesh, boundary conditions, etc.), this difference is significant. Figures 17 (a) and (b) show the gage pressure profiles just next to the main and pilot domes. Especially for the main dome region, the AUSM scheme predicts much smaller pressure, which indicates a much stronger PVC.

Based on these observations, we can expect that the JST scheme and the AUSM scheme would predict flame structures in a different manner, which is our ongoing work.

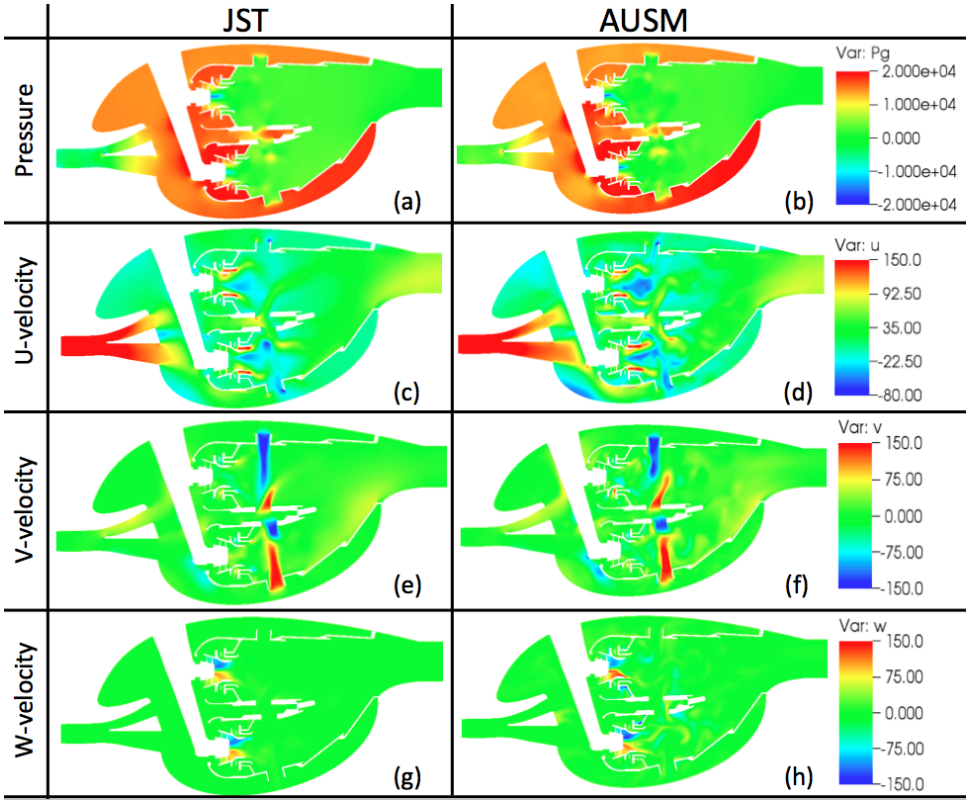


**Figure 13. Contours of gage pressure, u-velocity, v-velocity and w-velocity at the mid-plane using the JST scheme (left) and the AUSM scheme (right).**

## V. Conclusion

In this work, we have performed detailed validation studies of the newly implemented numerical schemes and applied them to the real combustor configuration, $E^3$ combustor. Compared with the available analytical solution & experimental data, the enhanced OpenNCC shows satisfactory performance. In the study of the $E^3$

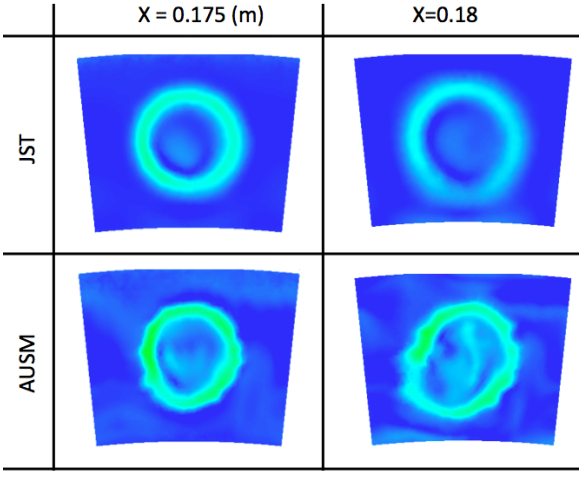


**Figure 14. Contours of Mach number at x=0.175 [m] and 0.18 [m] (blue: Mach = 0 and green: Mach =0.2).**

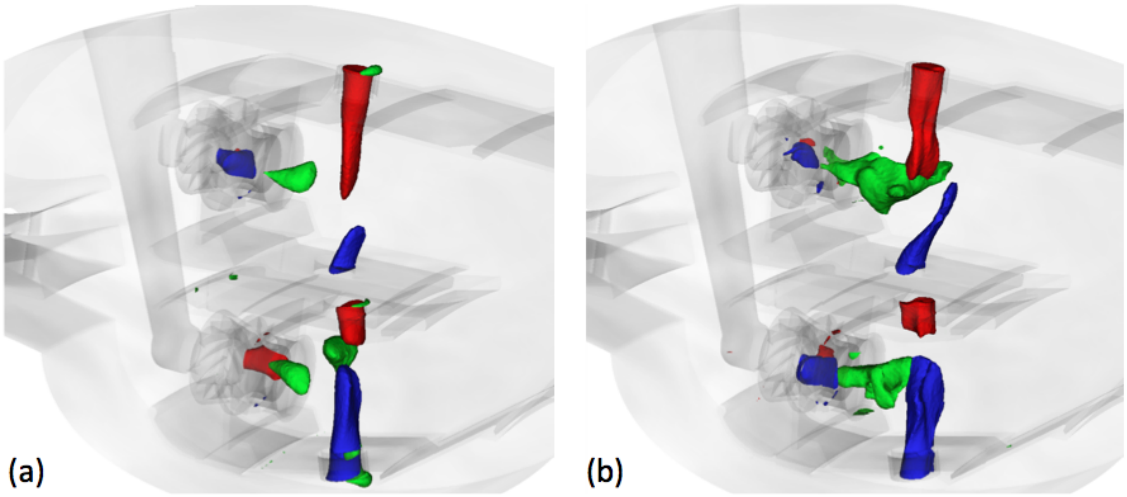


**Figure 15. Iso-surface of u-velocity (green: -30 [m/s]) and v-velocity (red:-100 [m/s], and blue: 100 [m/s]) using (a) JST scheme and (b) AUSM scheme.**

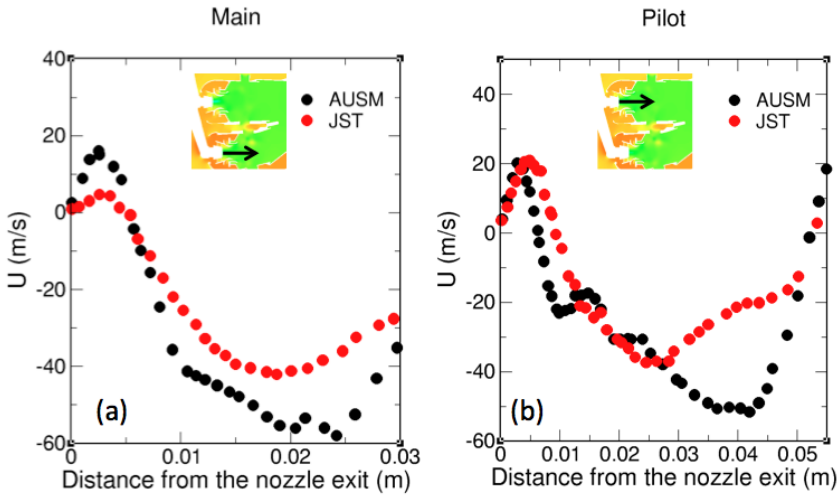


**Figure 16. U-velocity profile near the main dome (a) and the pilot dome (b)**

combustor, which is one of the most complicated CFD geometries publicly available, the preliminary results show that the choice of the numerical scheme might play a critical role in the accurate flow predictions, which could significantly influence the flame structure in a reacting flow case. From our exercise, we observe that the AUSM scheme is less dissipative and seems to capture the swirling flow and the recirculation buddle more realistically than the JST scheme. However, in terms of computational cost, the JST scheme is less expensive using a larger time step without numerical instability. Future work will involve the sensitivity analysis of combustion characteristics on the numerics and mesh quality in the $E^3$ combustor.

## References

[1]Gicquel, L. Y., Staffelbach, G., and Poinsot, T., "Large Eddy Simulations of gaseous flames in gas turbine combustion chambers," *Progress in Energy and Combustion Science*, Vol. 38, 2012, pp. 782–817.

[2]Stubbs, R. and Liu, N.-S., "Preview of the National Combustion Code," *33rd AIAA Joint Propulsion Conference*, No. AIAA 1997-3114, Seattle, WA, July 1997.

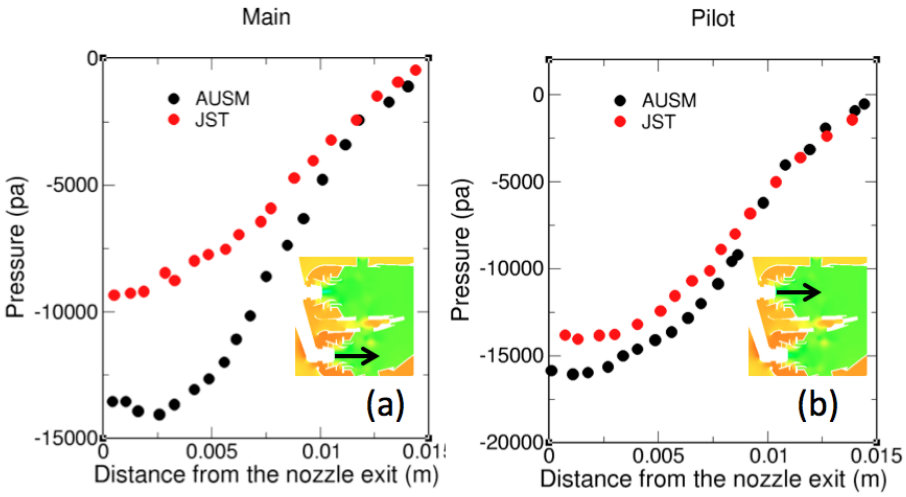


**Figure 17. Gage pressure profile near the main dome (a) and the pilot dome (b)**

[3]Shih, T.-H., Chen, K.-H., and Liu, N.-S., "A Non-linear k-epsilon Model for Turbulent Shear Flows," *34th AIAA/ASME/SAE/ASEE Joint Propulsion Conference & Exhibit*, No. AIAA 1998-35684, Cleveland, OH, July 13-15 1998.

[4]Raju, M., "A Lagrangian Spray solver - User's manual," No. NASA/CR97-206240, 1997.

[5]Raju, M., "An Eulerian-Based Monte Carlo Probability Density Function (PDF) Solver - User's manual," No. NASA/CR1998-20401, 1998.

[6]Raju, M., "LSPRAYII: A Lagrangian Spray Module," No. NASA/CR2004-212958, 2004.

[7]Liou, M.-S. and Steffen, C. J., "A new flux splitting scheme," *Journal of Computational Physics*, Vol. 107, 1993.

[8]Liou, M.-S., "A Sequel to AUSM: AUSM+," *Journal of Computational Physics*, Vol. 129, 1996.

[9]Liou, M.-S., "A Sequel to AUSM, Part II: AUSM+-up," *Journal of Computational Physics*, Vol. 214, 2006.

[10]Spadaccini, L. J., Owen, F. K., and Bowman, D. T., "Influence of aerodynamic phenomena on pollutant formation in combustion," *UTRC*, No. EPA-600/2-76-247a, East Hartford, CT, September 1976.

[11]Ciepluch, C. C., Davis, D. Y., and Gray, D. E., "Results of NASA's Energy Efficient Engine Program," *Journal of Propulsion and Power*, Vol. 3, 1987.

[12]Burrus, D. L., Chahrour, C. A., Foltz, H. L., Sabia, P. E., Seto, S. P., and Taylor, J. R., "Energy Efficent Engine Combustor Test Hardware Detailed Design Report," No. NASA/CR-1984-168301, 1984.

[13]Halila, E. E., Lenahan, D. T., and Thomas, T. T., "Energy Efficent Engine High Pressure Turbine Test Hardware Detailed Design Report," No. NASA/CR-1982-167955, 1982.

[14]Chen, K.-H. and Liu, N.-S., "Evaluation of A Non-Linear Turbulence Modeling Using Mixed Volume Unstructured grids," *36th AIAA Aerospace Sciences Meeting and Exhibit*, No. AIAA 1998-0233, Reno, NV, January 12-15 1998.

[15]Iannetti, A. C. and Moder, J. P., "Comparing Spray Characteristics from Reynolds Averaged Navier-Stokes (RANS) National Combustion Code (NCC) Calculations Against Experimental Data for a Turbulent Reacting Flow," No. NASA/CR-2010-216735, 2010.

[16]Wey, T. and Liu, N.-S., "Updates to Simulation of a Single-Element Lean-Direct Injection Combustor Using Arbitrary Polyhedral Meshes," *AIAA*, Kissimmee, FL, Jan 2015, pp. AIAA 2015–0099.

[17]Kumud, A. and Chen, K.-H., "Unsteady-Flow Computations for the NCC," *AIAA*, Reno, NV, Jan 2001, pp. AIAA 2001–0972.

[18]Chen, K.-H., Norris, A. T., Quealy, A., and Liu, N.-S., "Benchmark Test Cases for the Nathional Combustion Code," *34th AIAA/ASME/SAE/ASEE Joint Propulsion Conference & Exhibit*, No. AIAA 1998-3855, Cleveland, OH, July 13-15 1998.

[19]Iannetti, A. C., Tacina, R., Jeng, S.-H., and Cai, J., "Towards Accurate Predic tion of Turbulent, Three-Dimensional, Recirculating Flows With the NCC," No. NASA/TM2001-210761, 2012.

[20]Wey, T. and Liu, N.-S., "Updates to Simulation of a Single-Element Lean-Direct Injection Combustor Using a Polyhedral Mesh Derived from Hanging-Node Elements," *AIAA*, National Harbor, Maryland, Jan 2014, pp. AIAA 2014–1385.

[21]Liou, W. and Shih, T.-H., "Bypass Transitional Flow Calculation using a Navier-Stokes solver and Two-equation models," No. NASA/CR-2000-209923, 2000.

[22]van Leer, B., "Towards the ultimate conservation difference scheme. V - A second-order sequel to Godunov's method," *Journal of Computational Physics*, Vol. 32, 1979.

[23]Arts, T., Lambert de Rouvroit, M., and Rutherford, A., "Aero-thermal investigation of a highly loaded transonic linear turbine guide vane cascade," *VKI Technocal Note*, Vol. 174, 1990.

[24]Gourdain, E., Duchaine, F., Gicquel, L., and Collado, E., "Advanced Numerical Simulation Dedicated to the Prediction of Heat Transfer in a Highly Loaded Turbine Guide Vane," *ASME Turbo Expo 2010*, No. GT2010-22793, Glasgow, UK, June 1418, 2010.

[25]Shih, T.-H. and Liu, N.-S., "Simulations of Gas Fueld Reacting Flow in A Confined Turbulent Diffusion Flame," Not published (private communication).

[26]Bradley, D., Gaskella, P., Gua, X, J., Lawesa, M., and Scotta, M. J., "Premixed turbulent flame instability and NO formation in a lean-burn swirl burner," *Combustion and Flame*, Vol. 115, 1998, pp. 515–538.

[27]Lee, S.-Y., Seo, S., Broda, J., Pal, S., and Santoro, R., "An experimental estimation of mean reaction rate and flame structure during combustion instability in a lean premixed gas turbine combustor," *Proceedings of the Combustion Institute*, Vol. 28, 2000, pp. 775–782.